

Article

Correlation between Laboratory-Accelerated Corrosion and Field Exposure Test for High-Strength Stainless Steels

Jinchao Jiao ¹, Yong Lian ^{1,*} , Zhao Liu ¹, He Guo ¹, Jin Zhang ¹, Yan Su ², Junpeng Teng ², Yiming Jin ² and Jinyan Chen ²

¹ Institute for Advanced Materials Technology, University of Science and Technology Beijing, Beijing 100083, China

² Southwest Institute of Technology and Engineering, Chongqing 400039, China

* Correspondence: liany09@126.com

Abstract: Equipment in a long-term marine atmosphere environment is prone to corrosion failure. Natural field exposure tests usually require a long time to obtain corrosion information. This study worked out a laboratory-accelerated corrosion test method that has a strong correlation with the natural environment test in Wanning, Hainan, and can be used as the basis for life assessment and the prediction of two high-strength stainless-steel materials. The mathematical model of corrosion weight loss of two high-strength stainless steels (3Cr13 and 00Cr12Ni10MoTi) was established by a field exposure test and a laboratory-accelerated corrosion test. Then, the correlation between the field exposure test and the laboratory-accelerated corrosion test was evaluated using qualitative and quantitative methods, and the acceleration ratio was calculated using the accelerated switching factor (ASF) method. The results show that: (1) The corrosion morphology of the two stainless steels after 15 days of laboratory-accelerated corrosion testing is similar to that obtained after two years of field exposure. (2) The value of gray correlation between the laboratory-accelerated corrosion test and the field exposure test is not less than 0.75. (3) The acceleration ratio of both stainless steels increases with the corrosion test time in the laboratory. The corrosion prediction models for the two stainless steels are $T_{3Cr13} = 6.234 t^{1.634}$ and $T_{00Cr12Ni10MoTi} = 55.693 t^{1.322}$, respectively.

Keywords: high-strength stainless steel; field exposure test; laboratory-accelerated corrosion; correlation; marine atmospheric environment



Citation: Jiao, J.; Lian, Y.; Liu, Z.; Guo, H.; Zhang, J.; Su, Y.; Teng, J.; Jin, Y.; Chen, J. Correlation between Laboratory-Accelerated Corrosion and Field Exposure Test for High-Strength Stainless Steels. *Materials* **2022**, *15*, 9075. <https://doi.org/10.3390/ma15249075>

Academic Editor: Jose M. Bastidas

Received: 31 October 2022

Accepted: 6 December 2022

Published: 19 December 2022

Publisher's Note: MDPI stays neutral with regard to jurisdictional claims in published maps and institutional affiliations.



Copyright: © 2022 by the authors. Licensee MDPI, Basel, Switzerland. This article is an open access article distributed under the terms and conditions of the Creative Commons Attribution (CC BY) license (<https://creativecommons.org/licenses/by/4.0/>).

1. Introduction

The exploration, collection and transportation of marine resources rely on offshore infrastructure and equipment. Due to the conditions of the marine environment, a large number of steel structural components of marine facilities are highly susceptible to corrosion [1–3]. Therefore, the development of high-strength, corrosion-resistant, low-cost materials, as well as reasonable structural design and material selection, has become one of the key technologies in the development of the infrastructure and equipment of marine facilities. High-load-bearing structural components require high-strength or even ultra-high-strength stainless-steel materials. Among the many types of stainless steels, martensitic stainless steel meets the requirements for high-strength structural components [4,5]. Currently, 13wt.% Cr-type martensitic stainless steel is the most used [6], but martensitic stainless steel contains a lot of carbides, so its corrosion resistance is not high [7–10]. Maraging stainless steel is a new series developed on the basis of maraging steel from the late 1960s. In addition to its high strength, high toughness, easy processing and forming, simple heat treatment and good welding performance of maraging steel [11–13], it also has excellent corrosion resistance [14,15].

It is essential to carry out research on the corrosion mechanism and regularity of stainless steel in the marine atmospheric environment. The traditional research method

is the field exposure test in a natural environment [16], but due to the long period of the field exposure test, slow data recovery and the need for large manpower and material resources, the development of new corrosion-resistant materials has been severely limited [17]. Therefore, researchers expect to obtain atmospheric corrosion behavior and laws of materials in a relatively short period of time and predict the corrosion process of long-term outdoor exposure through short-term corrosion test results. At present, the most widely used is the laboratory-accelerated method, including the salt spray test [18–20], the wet–dry cycle immersion test [21–26], the cyclic corrosion test [27–29], etc. Whether the laboratory-accelerated test method is suitable for the studied material needs to be analyzed by correlating and establishing the connection between it and the external field exposure test [20,30–32]. The cyclic corrosion test includes three factors: salt spray, damp heat and dryness, which can better simulate the changes in the natural environment of the ocean atmosphere.

In this paper, martensitic stainless steel 3Cr13 and maraging stainless steel 00Cr12Ni10MoTi are the research objects. First, the corrosion weight-loss data of both stainless steels were obtained through the field exposure test and the laboratory-accelerated corrosion test. The laboratory-accelerated test parameters are based on the actual meteorological conditions in Wanning, Hainan, and the conversion method of the equivalent corrosion rate, which is the environmental load spectrum of Wanning, Hainan. The correlation between the laboratory-accelerated corrosion test and the field exposure test was then evaluated by qualitative and quantitative methods. Finally, the acceleration ratio of the laboratory-accelerated corrosion test to the two stainless-steel materials was calculated, and a corrosion-life prediction model based on the laboratory-accelerated corrosion test was established.

2. Materials and Methods

2.1. Materials

The experimental materials are martensitic stainless steel 3Cr13 (a commercial stainless steel offered by Daye Special Steel Co., Ltd., Huangshi, China) and maraging stainless steel 00Cr12Ni10MoTi, and their chemical components are shown in Table 1. Maraging stainless steel 00Cr12Ni10MoTi was prepared with low residual impurities in a 2-ton vacuum induction furnace, followed by vacuum arc remelting (Consarc, Inductotherm Group, Rancocas, NJ, USA). The heat treatment state and sample size of the two stainless steels are shown in Table 2. Before the start of the test, all samples were washed with absolute ethanol and dried with cold air, and the mass of the samples was weighed using an electronic balance (Mettler Toledo XPE1203S, Greifensee, Switzerland).

Table 1. Chemical composition content of two high-strength stainless steels (wt.%).

Material	C	Cr	Mo	Ni	Ti	Mn	Si	P	S	Fe
3Cr13	0.25–0.34	12.0–14.0	/	≤0.6	/	≤0.6	≤0.6	≤0.030	≤0.030	Bal.
00Cr12Ni10MoTi	≤0.03	11.0–13.0	0.5–2.0	9.5–12.0	0.8–2.0	/	/	≤0.015	≤0.015	Bal.

Table 2. Sample state and size.

Material	Heat Treatment	Sample Size
3Cr13 00Cr12Ni10MoTi	Quenching at 980 °C and tempering at 540 °C Solution at 980 °C and aging at 510 °C	100 mm × 50 mm × 3 mm

The specimens were polished to 2000# step by step using metallographic sandpaper and then polished with 1 μm grit diamond polish. 3Cr13 and 00Cr12Ni10MoTi were etched with 10% FeCl₃ solution and Ralph reagent (100 mL H₂O + 200 mL CH₃OH + 100 mL HCl + 2 g CuCl₂ + 7 g FeCl₂ + 5 mL HNO₃), respectively, and then metallographic photographs were taken using a metallographic microscope (Olympus Gx51, Tokyo, Japan).

All chemical reagents used in the experiments were purchased from Sinopharm Chemical Reagent Co., Ltd., Shanghai, China.

2.2. Field Exposure Test

The field exposure test was conducted in accordance with the “GB/T 14165-2008 experimental standard”. The test station is located in Wanning City, Hainan Province, along the coast of Shangen Town, longitude 110°05' E, latitude 18°58' N, altitude 12.3 m. The annual average temperature and relative humidity are 23.9 °C and 85%, respectively. The annual sunshine duration is 2005 h, and the rainfall pH is 5.0. It is a typical high-temperature and high-humidity marine atmospheric environment. There were four groups of samples and corrosion times (0.5, 1, 1.5 and 2 years), with three samples in each group.

2.3. Laboratory-Accelerated Corrosion Test

The laboratory-accelerated corrosion test consists of three stages of salt spray, drying and damp heat. The detailed parameters of each stage are shown in Table 3. The experimental equipment model was the JX-FH-90 salt spray chamber (Jiaxi Experimental Instrument Co., Ltd., Shanghai, China). There were five groups of samples and corrosion times (3, 6, 9, 12 and 15 days), with three samples in each group.

Table 3. Laboratory-accelerated test conditions.

Step	Duration Time (h)	Temperature (°C)	Relative Humidity	Solution (wt.%)
Salt spray	16	40	/	5% NaCl + 0.1% Na ₂ SO ₄ pH = 4
Dry	1	60	<30%	/
Wet	7	40	90%	/

3. Results

3.1. Microstructure

Figure 1 shows the microstructures of two high-strength stainless steels. 3Cr13 martensitic stainless steel belongs to medium-carbon steel. After quenching, a mixed structure of lath (dislocation) martensite and flake (twin) martensite is obtained. During the tempering process, alloy carbides such as (Cr, Fe)₇C₃ are precipitated from the martensite structure to form a tempered troostite structure composed of an α phase and granular carbides that retain the characteristics of the original martensite (Figure 1a). 00Cr12Ni10MoTi maraging stainless steel is an ultra-low carbon stainless steel, and a lath martensite structure with high dislocation density can be obtained by solution treatment. After the aging treatment, the matrix structure still retains lath-like characteristics (Figure 1b). A small amount of massive austenite structure is found at the grain boundary, and the aging precipitates are small and cannot be identified in the metallographic structure.

Figure 2 shows the typical TEM microstructure and diffraction pattern of 00Cr12Ni10MoTi martensitic stainless steel after aging treatment at 510 °C. It can be seen from the bright-field image (Figure 2a) that a large number of needle-like precipitates are precipitated in the martensite matrix after aging treatment. The precipitation phase is a hexagonal crystal structure intermetallic compound η -Ni₃Ti. Figure 2b is the dark-field image, with the arrow pointing to spot $(22\bar{4}0)_\eta$ in Figure 2c. The transmitted dark-field image clearly shows that the rod-shaped precipitates are dispersed in the lath martensite. The average diameter and length of the precipitates were about 3 nm and 12 nm, respectively. Figure 2d shows the complete diffraction pattern of the incident $[011]_{\alpha'}$ crystal band. The diffraction spots are indexed and calibrated. It can be found that the $(22\bar{4}0)$ diffraction spots of the precipitates and the $(\bar{2}20)$ diffraction spots of the matrix are in a straight line, which indicates that η -Ni₃Ti has the following orientation relationship with the martensite matrix:

$$(011)_M // (0001)_\eta, [\bar{2}22]_M // (22\bar{4}0)_\eta$$

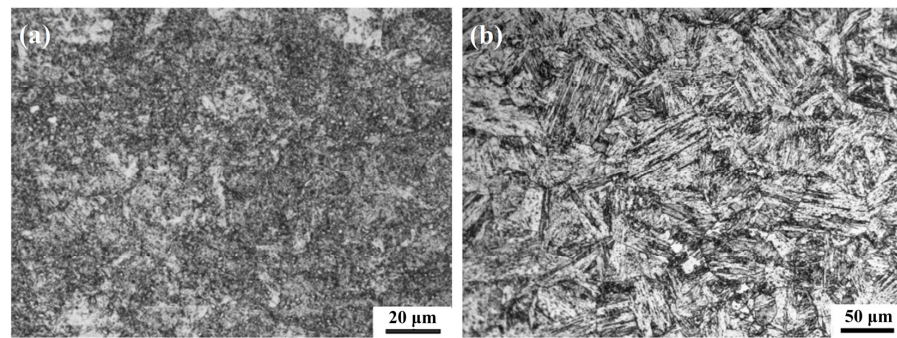


Figure 1. Microstructure of two materials: (a) 3Cr13 martensitic stainless steel tempered at 540 °C, (b) 00Cr12Ni10MoTi martensitic stainless steel aged at 510 °C.

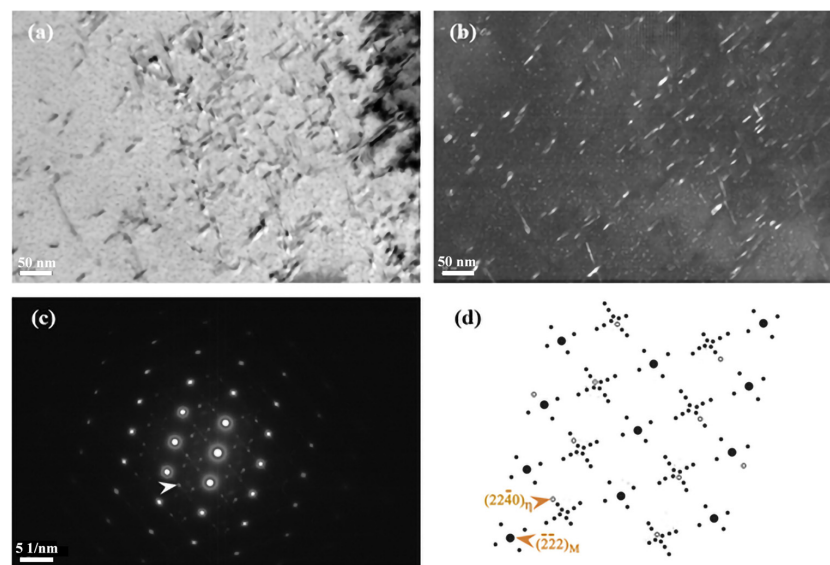


Figure 2. TEM photo of 00Cr12Ni10MoTi maraging stainless steel aged at 510 °C for 4 h: (a) bright-field image, (b) dark-field image taken from the diffraction spot indicated by an arrow in (c) showing precipitates, (c) selected area diffraction pattern with zone axis $[011]_{\alpha'}$, (d) schematics of selected area diffraction pattern with zone axis $[011]_{\alpha'}$.

3.2. Corrosion Weight-Loss Kinetics

The corrosion weight-loss data of 3Cr13 and 00Cr12Ni10MoTi stainless steels in the field-exposure corrosion test and laboratory-artificial accelerated test are shown in Tables 4 and 5, respectively. It can be seen that the corrosion weight loss of 00Cr12Ni10MoTi stainless steel is much smaller than that of 3Cr13 stainless steel in both test environments. As shown in Table 4, the corrosion weight loss of 3Cr13 martensitic stainless steel under the same exposure time is two orders of magnitude higher than that of 00Cr12Ni10MoTi maraging stainless steel, about 350 times.

Table 4. Corrosion weight-loss data of two stainless steels in natural environment.

Exposure Time (Years)	Corrosion Weight Loss ($\text{g}\cdot\text{m}^{-2}$)	
	3Cr13	00Cr12Ni10MoTi
0.5	112.594	0.321
1.0	195.689	0.566
1.5	334.926	0.849
2.0	387.453	1.094

Table 5. Corrosion weight-loss data of two stainless steels in laboratory artificially accelerated environment.

Accelerated Test Time (Days)	Corrosion Weight Loss ($\text{g}\cdot\text{m}^{-2}$)	
	3Cr13	00Cr12Ni10MoTi
3	28.087	0.435
6	66.000	0.783
9	114.000	1.478
12	222.870	2.000
15	322.783	2.870

The power function relationship model was used to fit the corrosion weight loss of the two materials in the natural environment test and the corrosion weight loss under the artificial acceleration test with time. A large number of studies have proved that the atmospheric corrosion kinetic equation of the power function model can reliably predict long-term corrosion. The empirical equation of the power function is as follows [33–36]:

$$D = At^n \quad (1)$$

where D is the corrosion weight loss (g/m^2), t is the corrosion time (h), and A and n are constants. The value of n can reflect the characteristics of corrosion kinetics, that is, $n > 1$ represents the corrosion acceleration process, $n < 1$ represents the corrosion deceleration process and $n = 1$ represents the uniform corrosion process [35,37].

Figure 3 shows the corrosion weight loss of two stainless steels with time and their fitting curves. D1 and D2 (Figure 3a) represent the fitting curves of the external field exposure corrosion weight loss and laboratory-accelerated corrosion weight loss of 3Cr13 martensitic stainless steel, respectively. D3 and D4 (Figure 3b) represent the fitting curves of the external field exposure corrosion weight loss and laboratory-accelerated corrosion weight loss of 00Cr12Ni10MoTi maraging stainless steel, respectively. The corresponding fitting equations are shown in Table 6. It can be seen that, under the field-exposed condition, the corrosion rate of both stainless steels decreases with time because their n values are less than 1. It should be noted that the 3Cr13 stainless steel is nearly uniformly corroded. In laboratory-accelerated corrosion, since the n value is greater than one, the corrosion rate of both stainless steels increased with time. It is shown that the laboratory acceleration method has an obvious acceleration effect on the two materials, and the decelerated corrosion process of external field exposure corrosion is transformed into an accelerated corrosion process. The reason may be that the short-term salt spray dry–wet alternation process during the accelerated corrosion process in the laboratory is not conducive to the “dissolution–reprecipitation” process of the corrosion product, which reduces the density of the corrosion product film, thereby reducing the corrosion product film’s protective effects. It can be seen from both field exposure and laboratory acceleration that the corrosion resistance of 00Cr12Ni10MoTi maraging stainless steel is better than that of 3Cr13 martensitic stainless steel in the atmospheric corrosion environment of Wanning, Hainan.

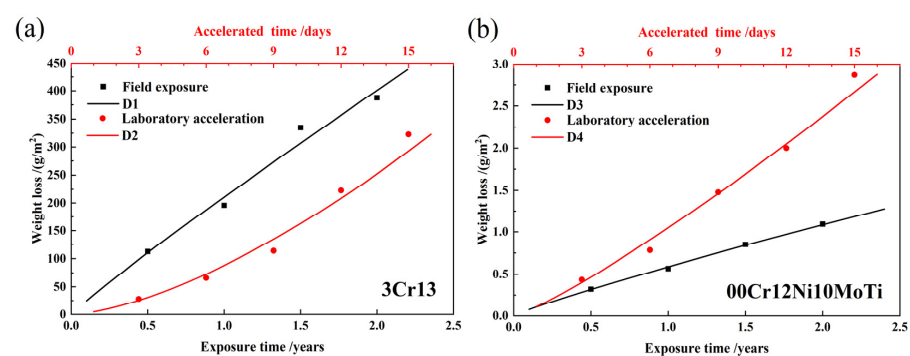
**Figure 3.** Field exposure and laboratory-accelerated corrosion weight loss of two materials with time and their fitting curves: (a) 3Cr13, (b) 00Cr12Ni10MoTi.

Table 6. Corrosion kinetic equations of two stainless steels.

Material	Experimental Conditions	Functional Model	Unit of t	R ²
3Cr13	Field exposure	$D1 = 210.470 t^{0.929}$	years	0.985
	Laboratory acceleration	$D2 = 4.780 t^{1.518}$	days	0.984
00Cr12Ni10MoTi	Field exposure	$D3 = 0.586 t^{0.889}$	years	0.998
	Laboratory acceleration	$D4 = 0.110 t^{1.177}$	days	0.984

3.3. Corrosion Morphology

Figure 4 shows the corrosion morphologies of two stainless steels, 3Cr13 and 00Cr12Ni10MoTi, after being exposed to corrosion for 0.5 and 2 years. It can be seen that the surface of 3Cr13 was completely covered by corrosion products after half a year of corrosion (Figure 4a), and there were network cracks in the corrosion products. After two years of corrosion (Figure 4b), there was no obvious cracking on the surface of the corrosion product. 00Cr12Ni10MoTi had only a small amount of corrosion products of different sizes on the surface after being corroded for half a year (Figure 4c), showing obvious pitting corrosion characteristics. After two years of corrosion (Figure 4d), pitting pits could be observed on the surface of the sample, and there was a small amount of corrosion products around the pits. Therefore, from the appearance of corrosion products, the corrosion resistance of maraging stainless steel 00Cr12Ni10MoTi is better than that of martensitic stainless steel 3Cr13.

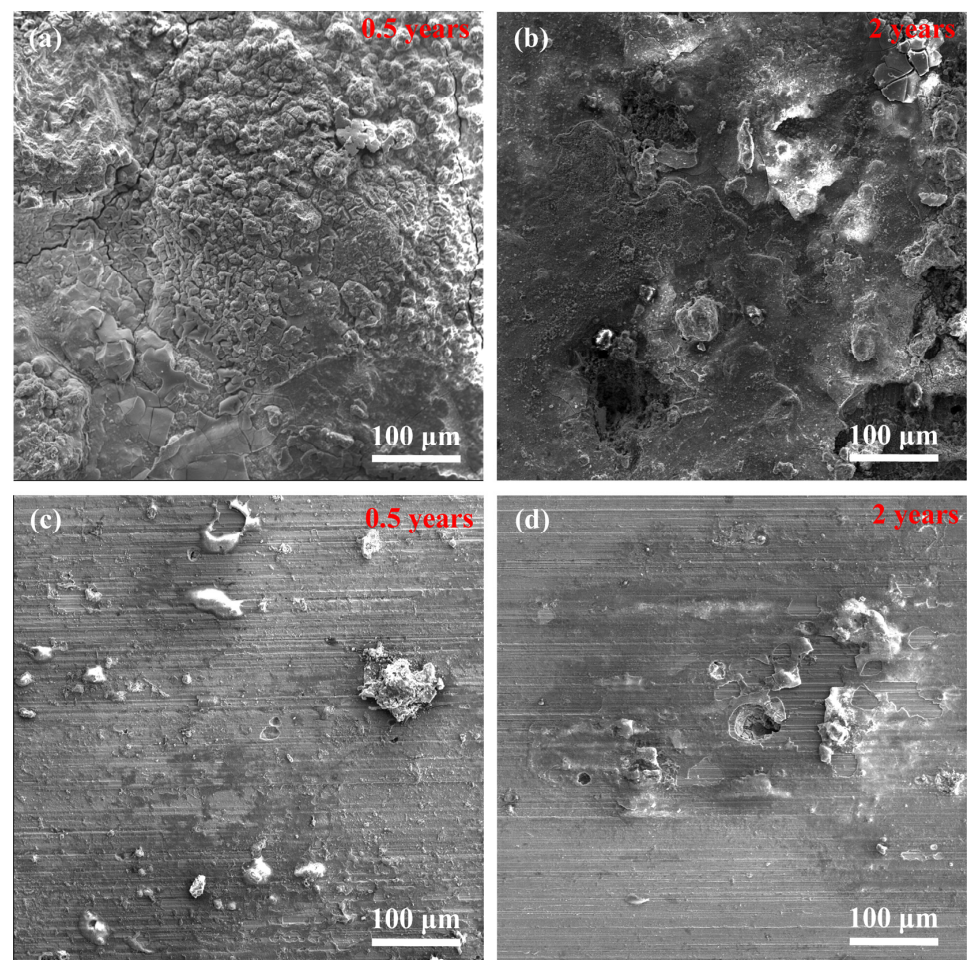


Figure 4. Corrosion microscopic morphology of two stainless steels after field exposure for different times: (a,b) 3Cr13, (c,d) 00Cr12Ni10MoTi.

3.4. Corrosion Products

Figure 5 shows the XPS spectra of Fe 2p_{3/2} and Cr 2p_{3/2} of the corrosion products of two stainless steels. Figure 5a,c show the peak fitting results of the XPS spectrum of Fe 2p_{3/2}. The spectrum of Fe 2p_{3/2} can be divided into three peaks, which are Fe²⁺ oxides, Fe³⁺ oxides and Fe³⁺ hydrated oxides. The corresponding corrosion products are FeO (710.7 eV), Fe₂O₃ (712.3 eV) and FeOOH (713.6 eV) [38]. Compared with 3Cr13, the FeO and Fe₂O₃ contents of 00Cr12Ni10MoTi are increased. The anodic reactions are as follows:

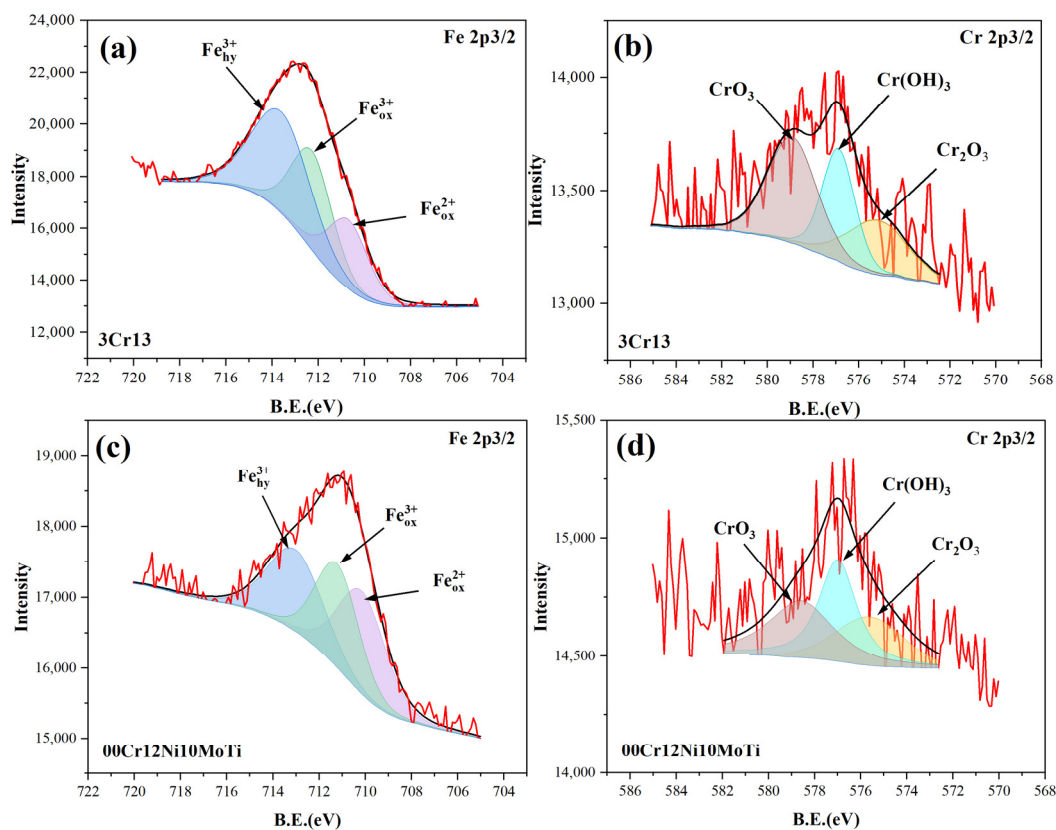
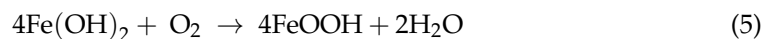
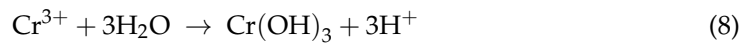


Figure 5. XPS spectra of corrosion products of two stainless steels corroded for two years: (a,b) 3Cr13, (c,d) 00Cr12Ni10MoTi.

Figure 5b,d show the peak fitting results of the XPS spectrum of Cr 2p_{3/2}. Cr₂O₃ (575.2 eV), Cr(OH)₃ (577.0 eV) and CrO₃ (578.6 eV) are the main forms of Cr in corrosion products [39–41]. Compared with 3Cr13, the contents of Cr₂O₃ and Cr(OH)₃ in 00Cr12Ni10MoTi increased significantly. Chromium plays an important role in the corrosion resistance of stainless steel, and chromium oxides are the main components of the passive film. The strength of Cr₂O₃ in 00Cr12Ni10MoTi is higher than that in 3Cr13, which improves the corrosion resistance. The formation of Cr(OH)₃ and Cr₂O₃ is as follows [41]:





Pitting corrosion is the most common corrosion type in high-strength stainless steel, and always occurs in the weak areas of passivation film, such as inclusions and carbide/intermetallic compound interfaces [42]. At the same time, the carbide precipitation in martensitic stainless steel causes local chromium depletion, which easily leads to intergranular corrosion [43]. Therefore, the difference in the corrosion resistance of the two stainless steels is related to their microstructure. During the tempering process of 3Cr13 martensitic stainless steel, alloy carbides such as $(\text{Cr, Fe})_7\text{C}_3$ precipitate from the martensitic structure, resulting in the existence of a Cr-depleted zone in the carbide boundary region [44]. Martensitic stainless steels passivate spontaneously by forming an oxide layer consisting mainly of Fe and Cr, so the precipitation of Cr-rich carbides reduces the passivation film and pitting resistance [6,7,10,45–47]. In the presence of aggressive anions (especially chloride ions), the breakdown of the passivation film causes the exposed metal to dissolve and thus form corrosion pits [6,7]. A corrosion cell is formed between the corrosion pit (anode) and the passivation film (cathode) surrounding the pit. After the aging treatment, the 00Cr12Ni10MoTi martensitic stainless steel has a lath martensite structure with a small amount of reversed austenite. There are a large number of nano-scale intermetallic compounds of $\eta\text{-Ni}_3\text{Ti}$ dispersed in the lath martensite, which will not form chromium-rich carbides. The formation of reversed austenite reduces the consumption of Cr around the carbide and the appearance of the Cr-depleted zone, which, in turn, enhances the passive film stability and pitting resistance [48,49]. In addition, the high content of Ni and Mo in the reversed austenite is beneficial to improve the pitting resistance in the austenite zone [50]. It has been reported that Ni can positively shift the pitting potential of stainless steel and contribute to the formation of Cr_2O_3 in the passivation film [51,52]. Therefore, 00Cr12Ni10MoTi martensitic stainless steel has better corrosion resistance in the specified environment.

4. Correlation Analysis

4.1. Qualitative Analysis

Qualitative analysis was performed using the method of macroscopic morphological comparison of corrosion specimens. The specimens exposed to corrosion in the external field for 2 years and the specimens exposed to accelerated corrosion in the laboratory for 15 days were selected for appearance comparison. As shown in Figure 6, when comparing the macroscopic corrosion morphology of the specimens under the two experimental environments, it can be seen that the surface of 3Cr13 martensitic stainless steel is covered by corrosion products, while the surface of 00Cr12Ni10MoTi martensitic stainless steel presents uniformly distributed pitting corrosion products. As the laboratory-accelerated corrosion accelerated the corrosion process, and due to the high moisture in the test chamber, a large number of liquefied solutions form the corrosion products and flow more obviously. Therefore, from the perspective of corrosion, the macroscopic morphology of laboratory-accelerated corrosion and external-exposure corrosion has a good consistency. The macroscopic corrosion morphology also indicates that the corrosion resistance of 00Cr12Ni10MoTi martensitic stainless steel is better than that of 3Cr13 martensitic stainless steel.

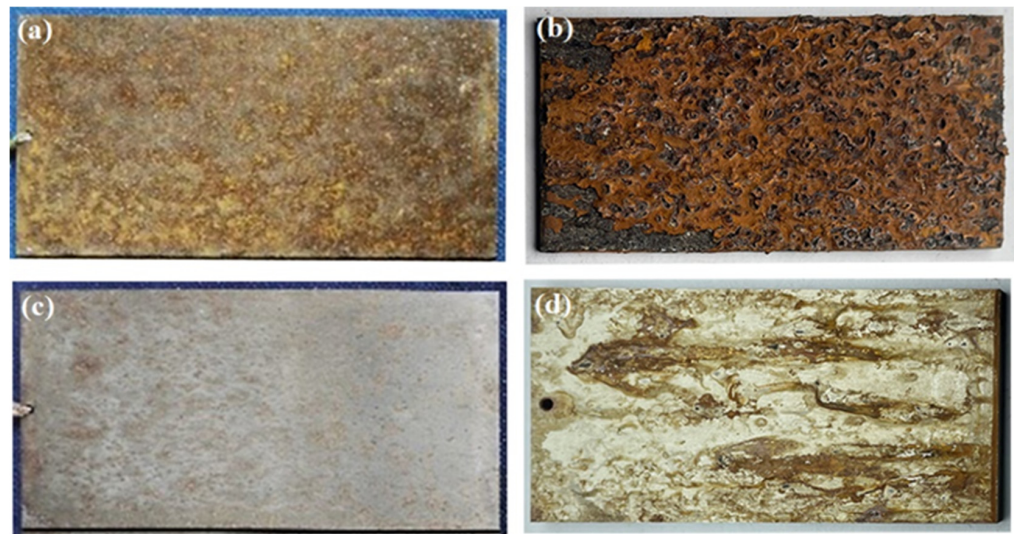


Figure 6. Comparison of corrosion morphology of two materials. Field exposure corrosion test for 2 years (a) and laboratory-accelerated corrosion test for 15 days (b) with 3Cr13; field exposure corrosion test for 2 years (c) and laboratory-accelerated corrosion test for 15 days (d) with 00Cr12Ni10MoTi.

4.2. Quantitative Analysis

Gray correlation analysis is used to measure the degree of association between two factors or two systems [32,53]. In this work, it was used to analyze the correlation between the laboratory-accelerated and field exposure tests of two stainless steels.

The weight-loss data from the field exposure test were used as a reference series to calculate the correlation between the laboratory-accelerated corrosion test and the field exposure test [54]. The calculation formula is below:

$$\xi_i(k) = \frac{\min_i \min_k |x_0(k) - x_i(k)| + \rho \max_i \max_k |x_0(k) - x_i(k)|}{|x_0(k) - x_i(k)| + \rho \max_i \max_k |x_0(k) - x_i(k)|} \quad (10)$$

where ρ is the resolution factor, which is generally set to 0.5. The calculation is performed using the homogenization method. The calculation results are shown in Table 7.

Table 7. Grey correlation between laboratory-accelerated and field exposure test.

Material	Raw Weight Loss ($\text{g}\cdot\text{m}^{-2}$)		Homogenization		Correlation Degree ξ_i	Mean
	Field Exposure	Laboratory-Accelerated	Field Exposure	Laboratory-Accelerated		
3Cr13	112.594	28.087	0.437	0.261	0.94	0.82
	195.689	66.000	0.759	0.613	1.00	
	334.962	114.000	1.300	1.058	0.82	
	387.453	222.870	1.504	2.069	0.51	
00Cr12Ni10MoTi	0.321	0.435	0.454	0.152	1.00	0.75
	0.566	0.783	0.800	0.273	0.76	
	0.849	1.478	1.200	0.515	0.66	
	1.094	2.000	1.546	0.697	0.57	

In general, when the gray correlation is greater than 0.6, the sequence is considered to be closely related to the reference sequence [32]. From Table 7, the gray correlation values between the laboratory-accelerated experiments and the external exposure tests for 3Cr13 martensitic stainless steel and 00Cr12Ni10MoTi martensitic stainless steel are 0.82 and 0.75, respectively, indicating a good correlation.

In summary, the study by qualitative and quantitative analysis showed a good correlation between the accelerated-laboratory test and the external field exposure test.

4.3. Acceleration Ratio Analysis

The accelerated conversion factor (ASF) method was used to calculate the acceleration ratio. The corrosion weight-loss data obtained in the laboratory-accelerated corrosion test were substituted into the kinetic equation of the field exposure test to calculate the time required for the field exposure test. Thereby, the relationship between the laboratory-accelerated corrosion time and the field exposure time was established. The calculation results are shown in Table 8.

Table 8. Relationship between laboratory-accelerated corrosion time and field exposure time for two stainless steels.

Material	Accelerated Time (Days)	Weight Loss (g·m ⁻²)	Functional Model	Time of Field Exposure (Days)
3Cr13	3	28.087	D1 = 210.470t ^{0.929}	42
	6	66.000		105
	9	114.000		189
	12	222.870		388
	15	322.783		578
00Cr12Ni10MoTi	3	0.435	D3 = 0.586t ^{0.890}	261
	6	0.783		505
	9	1.478		1032
	12	2.000		1450
	15	2.86957		2175

The function between the accelerated corrosion time and the field exposure time for the two stainless steels was obtained by regression analysis as:

$$T_{3Cr13} = 6.234 t^{1.634} \quad R^2 = 0.984 \tag{11}$$

$$T_{00Cr12Ni10MoTi} = 55.693 t^{1.322} \quad R^2 = 0.985 \tag{12}$$

where *t* is the laboratory acceleration time (days) and *T* is the field exposure time corresponding to *t* (days).

From this, the acceleration ratio of the two materials is deduced:

$$ASF_{3Cr13} = T_{3Cr13}/t = 6.234 t^{0.634} \tag{13}$$

$$ASF_{00Cr12Ni10MoTi} = T_{00Cr12Ni10MoTi}/t = 55.693 t^{0.322} \tag{14}$$

Equations (2)–(5) are plotted in Figure 7. From Figure 7b, it can be seen that the acceleration ratios of both 00Cr12Ni10MoTi and 3Cr13 increase with the increase in accelerated corrosion time. During this accelerated corrosion test, the acceleration ratio of 3Cr13 ranged from 0 to 50, and that of 00Cr12Ni10MoTi ranged from 50 to 150.

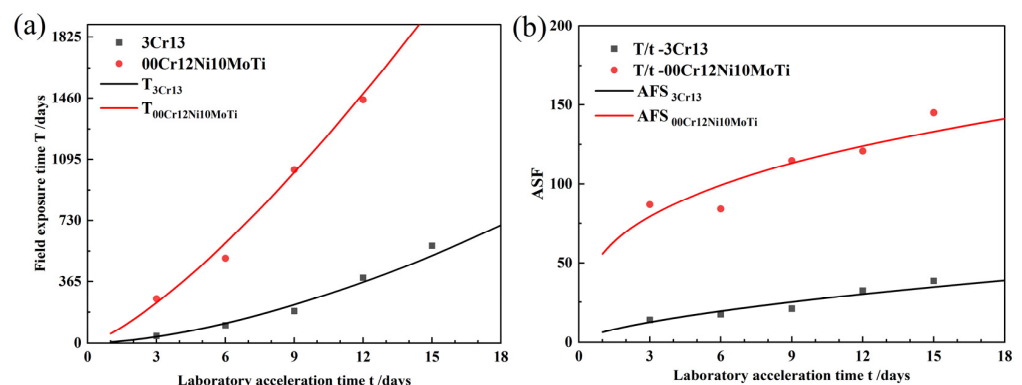


Figure 7. Acceleration ratio analysis: (a) relationship between laboratory-accelerated corrosion time and field exposure time, (b) acceleration ratio.

5. Conclusions

- (1) The corrosion resistance of 00Cr12Ni10MoTi martensitic stainless steel is greatly improved compared with that of 3Cr13 martensitic stainless steel, and the corrosion kinetics fitting curve is in accordance with the power function law.
- (2) Qualitative and quantitative analysis results show that the laboratory-accelerated corrosion test and the external field exposure test have a good correlation where the gray correlation coefficient is greater than 0.75. Therefore, the artificially accelerated corrosion method used in this study can be used as the basis for life assessment and the prediction of stainless-steel materials. The corrosion prediction models for the two stainless steels are $T_{3Cr13} = 6.234 t^{1.634}$ and $T_{00Cr12Ni10MoTi} = 55.693 t^{1.322}$, respectively.
- (3) The passivation film and corrosion product film formed on the surface of 00Cr12Ni10MoTi martensitic aging stainless steel has a protective effect, while the passivation film and corrosion product film on the surface of 3Cr13 martensitic stainless steel has a lower protective effect.

Author Contributions: Conceptualization, Y.L., Y.S. and J.Z.; methodology, Y.L., J.T. and J.J.; formal analysis, J.J.; data curation, Y.J., J.C., Z.L. and H.G.; writing—original draft preparation, J.J.; writing—review and editing, Y.L. and J.J.; visualization, J.J.; supervision, Y.L., Y.S. and J.T.; project administration, Y.L., Y.J. and J.C.; funding acquisition, Y.L. and J.Z. All authors have read and agreed to the published version of the manuscript.

Funding: This research was funded by the Southwest Institute of Technology and Engineering Cooperation Fund, grant number HDHDW5902020106.

Institutional Review Board Statement: Not applicable.

Informed Consent Statement: Not applicable.

Data Availability Statement: Not applicable.

Conflicts of Interest: The authors declare no conflict of interest.

References

1. Alcántara, J.; de la Fuente, D.; Chico, B.; Simancas, J.; Díaz, I.; Morcillo, M. Marine Atmospheric Corrosion of Carbon Steel: A Review. *Materials* **2017**, *10*, 406. [[CrossRef](#)] [[PubMed](#)]
2. Wood, R.J.K. Erosion–Corrosion Interactions and Their Effect on Marine and Offshore Materials. *Wear* **2006**, *261*, 1012–1023. [[CrossRef](#)]
3. Soares, C.G.; Garbatov, Y.; Zayed, A.; Wang, G. Influence of Environmental Factors on Corrosion of Ship Structures in Marine Atmosphere. *Corros. Sci.* **2009**, *51*, 2014–2026. [[CrossRef](#)]
4. Bonagani, S.K.; Kain, V.; Naveen Kumar, N.; Donthula, H. Effect of Austenitization-Cooling on Microstructure and Localized Corrosion Behavior of 13Cr Martensitic Stainless Steel. *J. Mater. Eng. Perform.* **2021**, *30*, 2291–2299. [[CrossRef](#)]
5. Derazkola, H.A.; García Gil, E.; Murillo-Marrodán, A.; Méresse, D. Review on Dynamic Recrystallization of Martensitic Stainless Steels during Hot Deformation: Part I—Experimental Study. *Metals* **2021**, *11*, 572. [[CrossRef](#)]
6. Lu, S.-Y.; Yao, K.-F.; Chen, Y.-B.; Wang, M.-H.; Liu, X.; Ge, X. The Effect of Tempering Temperature on the Microstructure and Electrochemical Properties of a 13wt.% Cr-Type Martensitic Stainless Steel. *Electrochim. Acta* **2015**, *165*, 45–55. [[CrossRef](#)]
7. Bonagani, S.K.; Bathula, V.; Kain, V. Influence of Tempering Treatment on Microstructure and Pitting Corrosion of 13 wt.% Cr Martensitic Stainless Steel. *Corros. Sci.* **2018**, *131*, 340–354. [[CrossRef](#)]
8. Radwan, A.B.; Moussa, A.M.; Al-Qahtani, N.H.; Case, R.; Castaneda, H.; Abdullah, A.M.; El-Haddad, M.A.M.; Bhadra, J.; Al-Thani, N.J. Evaluation of the Pitting Corrosion of Modified Martensitic Stainless Steel in CO₂ Environment Using Point Defect Model. *Metals* **2022**, *12*, 233. [[CrossRef](#)]
9. Landgraf, P.; Birnbaum, P.; Meza-García, E.; Grund, T.; Kräusel, V.; Lampke, T. Jominy End Quench Test of Martensitic Stainless Steel X30Cr13. *Metals* **2021**, *11*, 1071. [[CrossRef](#)]
10. Zhao, Y.; Liu, W.; Zhang, T.; Sun, Z.; Wang, Y.; Fan, Y.; Dong, B. Assessment of the Correlation between M23C6 Precipitates and Pitting Corrosion Resistance of 0Cr13 Martensitic Stainless Steel. *Corros. Sci.* **2021**, *189*, 109580. [[CrossRef](#)]
11. Vodárek, V.; Rožnovská, G.; Kuboň, Z.; Volodarskaja, A.; Palupčíková, R. The Effect of Long-Term Ageing at 475 °C on Microstructure and Properties of a Precipitation Hardening Martensitic Stainless Steel. *Metals* **2022**, *12*, 1643. [[CrossRef](#)]
12. Li, Y.; Yan, W.; Cotton, J.D.; Ryan, G.J.; Shen, Y.; Wang, W.; Shan, Y.; Yang, K. A New 1.9GPa Maraging Stainless Steel Strengthened by Multiple Precipitating Species. *Mater. Des.* **2015**, *82*, 56–63. [[CrossRef](#)]

13. Xu, W.; Rivera-Díaz-del-Castillo, P.E.J.; Yan, W.; Yang, K.; San Martín, D.; Kestens, L.A.I.; van der Zwaag, S. A New Ultrahigh-Strength Stainless Steel Strengthened by Various Coexisting Nanoprecipitates. *Acta Mater.* **2010**, *58*, 4067–4075. [[CrossRef](#)]
14. Almeraya-Calderón, F.; Samaniego-Gámez, O.; Maldonado-Bandala, E.; Nieves-Mendoza, D.; Olguín-Coca, J.; Jáquez-Muñoz, J.M.; Cabral-Miramontes, J.; Flores-De los Rios, J.P.; Bautista-Margulis, R.G.; Gaona-Tiburcio, C. Corrosion Behavior of Passivated Martensitic and Semi-Austenitic Precipitation Hardening Stainless Steel. *Metals* **2022**, *12*, 1033. [[CrossRef](#)]
15. Tian, J.; Wang, W.; Babar Shahzad, M.; Yan, W.; Shan, Y.; Jiang, Z.; Yang, K. A New Maraging Stainless Steel with Excellent Strength–Toughness–Corrosion Synergy. *Materials* **2017**, *10*, 1293. [[CrossRef](#)] [[PubMed](#)]
16. Cai, Y.; Xu, Y.; Zhao, Y.; Ma, X. Atmospheric Corrosion Prediction: A Review. *Corros. Rev.* **2020**, *38*, 299–321. [[CrossRef](#)]
17. Lin, C.-C.; Wang, C.-X. Correlation between Accelerated Corrosion Tests and Atmospheric Corrosion Tests on Steel. *J. Appl. Electrochem.* **2005**, *35*, 837–843. [[CrossRef](#)]
18. Zhu, S.; Liu, Z.; Qu, R.; Wang, L.; Li, Q.; Guan, S. Effect of Rare Earth and Mn Elements on the Corrosion Behavior of Extruded AZ61 System in 3.5 Wt% NaCl Solution and Salt Spray Test. *J. Magnes. Alloys* **2013**, *1*, 249–255. [[CrossRef](#)]
19. Pathak, S.S.; Blanton, M.D.; Mendon, S.K.; Rawlins, J.W. Investigation on Dual Corrosion Performance of Magnesium-Rich Primer for Aluminum Alloys under Salt Spray Test (ASTM B117) and Natural Exposure. *Corros. Sci.* **2010**, *52*, 1453–1463. [[CrossRef](#)]
20. Sun, X.; Lin, P.; Man, C.; Cui, J.; Wang, H.; Dong, C.; Li, X. Prediction Model for Atmospheric Corrosion of 7005-T4 Aluminum Alloy in Industrial and Marine Environments. *Int. J. Min. Met. Mater.* **2018**, *25*, 1313–1319. [[CrossRef](#)]
21. Yu, M.; Zu, H.; Zhao, K.; Liu, J.; Li, S. Effects of Dry/Wet Ratio and Pre-Immersion on Stress Corrosion Cracking of 7050-T7451 Aluminum Alloy under Wet-Dry Cyclic Conditions. *Chin. J. Aeronaut.* **2018**, *31*, 2176–2184. [[CrossRef](#)]
22. Yu, J.; Wang, H.; Yu, Y.; Luo, Z.; Liu, W.; Wang, C. Corrosion Behavior of X65 Pipeline Steel: Comparison of Wet–Dry Cycle and Full Immersion. *Corros. Sci.* **2018**, *133*, 276–287. [[CrossRef](#)]
23. Gong, K.; Wu, M.; Liu, G. Comparative Study on Corrosion Behaviour of Rusted X100 Steel in Dry/Wet Cycle and Immersion Environments. *Constr. Build. Mater.* **2020**, *235*, 117440. [[CrossRef](#)]
24. Calero, J.; Alcántara, J.; Chico, B.; Díaz, I.; Simancas, J.; de la Fuente, D.; Morcillo, M. Wet/Dry Accelerated Laboratory Test to Simulate the Formation of Multilayered Rust on Carbon Steel in Marine Atmospheres. *Corros. Eng. Sci. Technol.* **2017**, *52*, 178–187. [[CrossRef](#)]
25. Guo, J.-J.; Wang, K.; Guo, T.; Yang, Z.-Y.; Zhang, P. Effect of Dry–Wet Ratio on Properties of Concrete Under Sulfate Attack. *Materials* **2019**, *12*, 2755. [[CrossRef](#)] [[PubMed](#)]
26. Lian, X.; Zhu, J.; Wang, R.; Liu, T.; Xu, J.; Xu, D.; Dong, H. Effects of Rare Earth (Ce and La) on Steel Corrosion Behaviors under Wet-Dry Cycle Immersion Conditions. *Metals* **2020**, *10*, 1174. [[CrossRef](#)]
27. Bahrami, M.; Ranjbar, Z.; Khosroshahi, R.A.; Ashhari, S. Investigating Corrosion Protection Properties of Epoxy Thermal Insulators through Cyclic Corrosion Test. *Prog. Org. Coat.* **2017**, *113*, 25–30. [[CrossRef](#)]
28. Li, S.; Zhang, Z.; Akiyama, E.; Tsuzaki, K.; Zhang, B. Evaluation of Susceptibility of High Strength Steels to Delayed Fracture by Using Cyclic Corrosion Test and Slow Strain Rate Test. *Corros. Sci.* **2010**, *52*, 1660–1667. [[CrossRef](#)]
29. LeBozec, N.; Blandin, N.; Thierry, D. Accelerated Corrosion Tests in the Automotive Industry: A Comparison of the Performance towards Cosmetic Corrosion. *Mater. Corros.* **2008**, *59*, 889–894. [[CrossRef](#)]
30. Papadopoulos, M.P.; Apostolopoulos, C.A.; Zervaki, A.D.; Haidemenopoulos, G.N. Corrosion of Exposed Rebars, Associated Mechanical Degradation and Correlation with Accelerated Corrosion Tests. *Constr. Build. Mater.* **2011**, *25*, 3367–3374. [[CrossRef](#)]
31. Almusallam, A.A. Effect of Degree of Corrosion on the Properties of Reinforcing Steel Bars. *Constr. Build. Mater.* **2001**, *15*, 361–368. [[CrossRef](#)]
32. Wu, H.; Lei, H.; Chen, Y.F. Grey Relational Analysis of Static Tensile Properties of Structural Steel Subjected to Urban Industrial Atmospheric Corrosion and Accelerated Corrosion. *Constr. Build. Mater.* **2022**, *315*, 125706. [[CrossRef](#)]
33. Lan, T.T.N.; Thoa, N.T.P.; Nishimura, R.; Tsujino, Y.; Yokoi, M.; Maeda, Y. Atmospheric Corrosion of Carbon Steel under Field Exposure in the Southern Part of Vietnam. *Corros. Sci.* **2006**, *48*, 179–192. [[CrossRef](#)]
34. Corvo, F.; Perez, T.; Dzib, L.R.; Martin, Y.; Castañeda, A.; Gonzalez, E.; Perez, J. Outdoor–Indoor Corrosion of Metals in Tropical Coastal Atmospheres. *Corros. Sci.* **2008**, *50*, 220–230. [[CrossRef](#)]
35. Ma, Y.; Li, Y.; Wang, F. The Atmospheric Corrosion Kinetics of Low Carbon Steel in a Tropical Marine Environment. *Corros. Sci.* **2010**, *52*, 1796–1800. [[CrossRef](#)]
36. Lien, L.T.H.; San, P.T.; Hong, H.L. Results of Studying Atmospheric Corrosion in Vietnam 1995–2005. *Sci. Technol. Adv. Mater.* **2007**, *8*, 552–558. [[CrossRef](#)]
37. Ma, Y.; Li, Y.; Wang, F. Corrosion of Low Carbon Steel in Atmospheric Environments of Different Chloride Content. *Corros. Sci.* **2009**, *51*, 997–1006. [[CrossRef](#)]
38. Li, X.; Zhao, Y.; Qi, W.; Xie, J.; Wang, J.; Liu, B.; Zeng, G.; Zhang, T.; Wang, F. Effect of Extremely Aggressive Environment on the Nature of Corrosion Scales of HP-13Cr Stainless Steel. *Appl. Surf. Sci.* **2019**, *469*, 146–161. [[CrossRef](#)]
39. Zou, D.; Liu, R.; Li, J.; Zhang, W.; Wang, D.; Han, Y. Corrosion Resistance and Semiconducting Properties of Passive Films Formed on 00Cr13Ni5Mo2 Supermartensitic Stainless Steel in Cl– Environment. *J. Iron Steel Res. Int.* **2014**, *21*, 630–636. [[CrossRef](#)]
40. Zhang, W.; Zhang, X.; Qiao, G.; Zou, D.; Zhou, Y.; Shen, C. Effect of Cobalt on the Microstructure and Corrosion Behavior of Martensitic Age-Hardened Stainless Steel. *J. Mater. Eng. Perform.* **2019**, *28*, 4197–4208. [[CrossRef](#)]
41. Sun, M.; Xiao, K.; Dong, C.; Li, X.; Zhong, P. Electrochemical and Initial Corrosion Behavior of Ultrahigh Strength Steel by Scanning Kelvin Probe. *J. Mater. Eng. Perform.* **2013**, *22*, 815–822. [[CrossRef](#)]

42. Wang, L.; Dong, C.; Man, C.; Hu, Y.; Yu, Q.; Li, X. Effect of Microstructure on Corrosion Behavior of High Strength Martensite Steel—A Literature Review. *Int. J. Min. Met. Mater.* **2021**, *28*, 754–773. [[CrossRef](#)]
43. Hu, S.; Mao, Y.; Liu, X.; Han, E.-H.; Hänninen, H. Intergranular Corrosion Behavior of Low-Chromium Ferritic Stainless Steel without Cr-Carbide Precipitation after Aging. *Corros. Sci.* **2020**, *166*, 108420. [[CrossRef](#)]
44. Nakamichi, H.; Sato, K.; Miyata, Y.; Kimura, M.; Masamura, K. Quantitative Analysis of Cr-Depleted Zone Morphology in Low Carbon Martensitic Stainless Steel Using FE-(S)TEM. *Corros. Sci.* **2008**, *50*, 309–315. [[CrossRef](#)]
45. Dalmau, A.; Richard, C.; Igual-Muñoz, A. Degradation Mechanisms in Martensitic Stainless Steels: Wear, Corrosion and Tribocorrosion Appraisal. *Tribol. Int.* **2018**, *121*, 167–179. [[CrossRef](#)]
46. Marcelin, S.; Pébère, N.; Régner, S. Electrochemical Characterisation of a Martensitic Stainless Steel in a Neutral Chloride Solution. *Electrochim. Acta* **2013**, *87*, 32–40. [[CrossRef](#)]
47. Zhang, H.; Zhao, Y.L.; Jiang, Z.D. Effects of Temperature on the Corrosion Behavior of 13Cr Martensitic Stainless Steel during Exposure to CO₂ and Cl⁻ Environment. *Mater. Lett.* **2005**, *59*, 3370–3374. [[CrossRef](#)]
48. Wang, L.; Dong, C.; Yao, J.; Dai, Z.; Man, C.; Yin, Y.; Xiao, K.; Li, X. The Effect of η -Ni₃Ti Precipitates and Reversed Austenite on the Passive Film Stability of Nickel-Rich Custom 465 Steel. *Corros. Sci.* **2019**, *154*, 178–190. [[CrossRef](#)]
49. Song, Y.; Li, X.; Rong, L.; Li, Y. The Influence of Tempering Temperature on the Reversed Austenite Formation and Tensile Properties in Fe–13%Cr–4%Ni–Mo Low Carbon Martensite Stainless Steels. *Mater. Sci. Eng. A* **2011**, *528*, 4075–4079. [[CrossRef](#)]
50. Lei, X.; Feng, Y.; Zhang, J.; Fu, A.; Yin, C.; Macdonald, D.D. Impact of Reversed Austenite on the Pitting Corrosion Behavior of Super 13Cr Martensitic Stainless Steel. *Electrochim. Acta* **2016**, *191*, 640–650. [[CrossRef](#)]
51. Olsson, C.-O.A.; Landolt, D. Passive Films on Stainless Steels—Chemistry, Structure and Growth. *Electrochim. Acta* **2003**, *48*, 1093–1104. [[CrossRef](#)]
52. Cheng, X.; Jin, Z.; Liu, M.; Li, X. Optimizing the Nickel Content in Weathering Steels to Enhance Their Corrosion Resistance in Acidic Atmospheres. *Corros. Sci.* **2017**, *115*, 135–142. [[CrossRef](#)]
53. Liu, S.; Lin, Y. *Grey Systems Theory and Application; Understanding Complex Systems*; Springer: Berlin/Heidelberg, Germany, 2011; Volume 68, ISBN 978-3-642-16157-5.
54. Moutarlier, V.; Gigandet, M.P.; Normand, B.; Pagetti, J. EIS Characterisation of Anodic Films Formed on 2024 Aluminium Alloy, in Sulphuric Acid Containing Molybdate or Permanganate Species. *Corros. Sci.* **2005**, *47*, 937–951. [[CrossRef](#)]